Chapter 6

Regularization Techniques using Fuzzy POCS

6.1 Introduction

Post-processing techniques for the correction of rotational motion artifacts often involve interpolation and re-gridding of the acquired k-space data. These methods create significant data void regions in the corrected k-space. Projection onto convex sets (POCS) is used in the previous chapter, for estimating the missing k-space values in such regions. However, the quality of the POCS solution largely depends on *a priori* constraints used in forming the convex sets. It can be shown that the acquired k-space data are often subjected to noise, measurement errors and interpolation errors which cause the k-space constraints to form an ill defined convex set, inconsistent with the spatial constraints. Inconsistent constraints lead to the divergence of POCS from the desired solution, within a finite number of iterations. In this chapter, a fuzzy model is proposed for representing the reliability of available k-space values. This model is used for adaptive updating of the convex set during the POCS iterations. The updates are based

on the highly reliable k-space data and the consistency of the convex set with the spatial constraints. Therefore, the proposed fuzzy model avoids divergence of the POCS solution from the required result, and also ensures final image quality improvement.

6.2 Reliability of Convex Sets

Decades of research has established the fact that the quality of the POCS solution largely depends on *a priori* knowledge of the original form of the image and the accuracy of the signal degradation model. A major problem is utilizing all available knowledge optimally, since not all *a priori* knowledge is equally reliable.

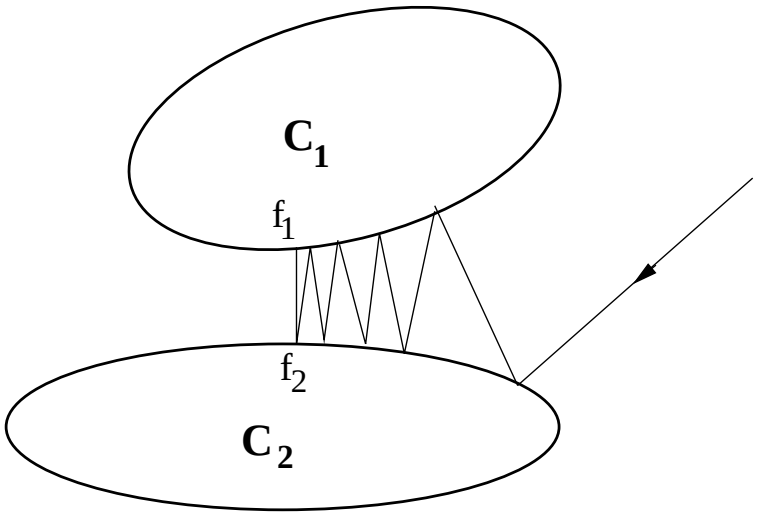

Figure 6.1: Projection between two non-intersecting convex sets results in a minimum mean square limit cycle. Point f_1 is the point in C_1 closest to C_2 and point f_2 is the point in C_2 closest to C_1.

In POCS, unreliable or inaccurate *a priori* information leads to inconsistent convex sets where the intersection is essentially empty. Inconsistent convex sets lead to slow convergence, and divergence from the desired solution, causing problems with the termination of iterations. If there are only two sets, the convergence is to the cycle between the closest points of the sets in the mean square sense. This

is illustrated in Figure 6.1. If there are more than two sets, POCS converge to greedy limit cycles that are dependent on the ordering of the projections [107]. Therefore, the final solution does not display all the expected properties. This is geometrically illustrated in Figure 6.2.

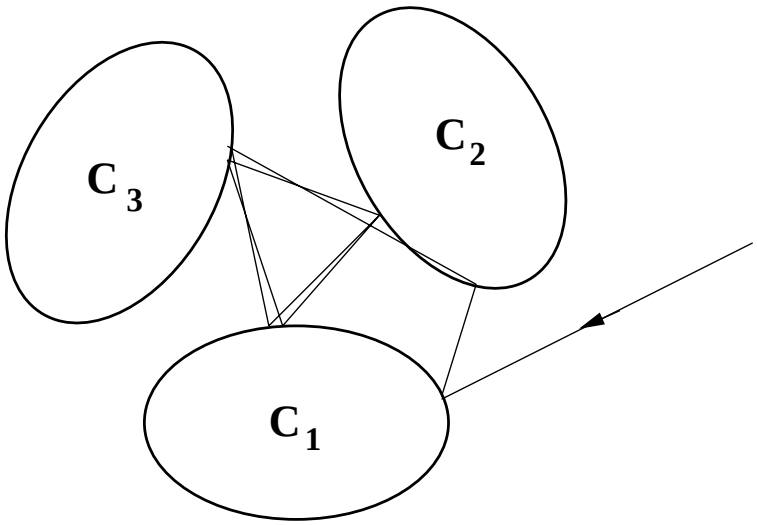

Figure 6.2: Projection between three or more non-intersecting convex sets results in greedy limit cycles. These cycles correspond to all the possible projection orders (eg. 123, 213, 321 etc.).

It was observed in Chapter 5, that the reconstructed image diverges from the desired image within a finite number of iterations, under certain circumstances. Therefore, a computationally expensive regulatory error metric E was used to determine the point of termination of iterations. The cause for such divergence is found to be the inconsistent k-space constraints imposed on the POCS algorithm. This inconsistency arises due to the noise, measurement errors and interpolation errors embedded in the available k-space data, that has been used for imposing k-space constraints. Spatial constraints can be affected by errors in estimation of the ROI and maximum energy. Rotation angle estimation errors are also demonstrated to cause k-space data errors, as shown in Chapter 5.

Each of the available spatial frequency values can lead to a separate convex set of the form of a linear variety in the Hilbert space. A linear variety is defined as

a translation of a subspace by a fixed vector [108]. This fixed vector is computed from the known spatial frequency value, and defines the location of a particular linear variety in the Hilbert space.

If the reliability of each computed k-space value is known, each resultant linear variety can be fuzzified with a membership function [137] determined by its reliability. Depending on its membership, each vector can be given freedom to move , so that a set of fuzzy linear varieties can be formed which do not contradict the spatial constraints defined in *a priori* spatial constraints. Therefore, proper fuzzification of linear varieties can transform inconsistent sets of constraints to a group of convex sets with a non-empty intersection. Such a result can be achieved by using the method of fuzzy POCS [103].

6.3 Fuzzy POCS

As shown in the previous section, POCS breaks down in the important case where two or more convex sets do not intersect [138]. However, regularization using fuzzy constraints [139] [140] can be applied to find valuable POCS solutions that are *close enough* to each of the convex constraints. The underlying concept of being *close enough* suggests fuzzification of the non-intersecting convex sets to fuzzy convex sets [131]. Even if two or more crisp convex sets do not intersect, α-cuts [131] of their corresponding fuzzy sets can. This is illustrated in Figure 6.3. Although fuzzy POCS often does not result in a fixed point solution, the extent of the limit cycle of convergence can be effectively reduced.

There are two methods of fuzzification of crisp convex sets, using dilation of the convex sets [103]. The amount of dilation is dependent on the reliability of the constraints used to form the convex set. The most reliable convex set should be

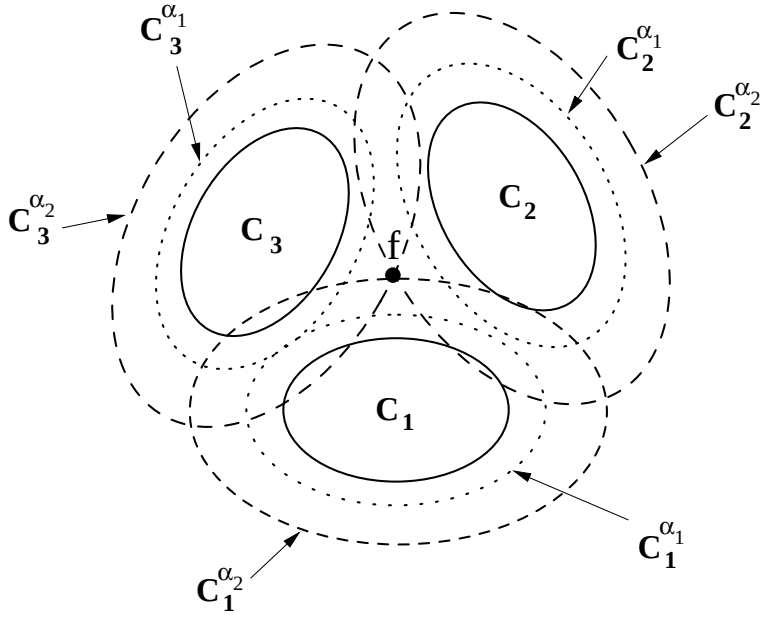

Figure 6.3: Three non-intersecting convex sets are fuzzified through morphological dilation. Shown contours are for two different α-cuts α_1 and α_2. At some combination of α-cuts, it is possible to force the contours to intersect at a point f, which is *close enough* to each of the three constraint sets.

dilated the least and the least reliable convex set should be dilated the most, in order to optimize the use of reliable information.

If a crisp convex set is parameterized, in many cases, the fuzzy convex set can be generated by fuzzification of the parameter set. If the parameter set exists on an interval (eg. $0 \leq Bandwidth \leq \Omega$ for a set of band-limited functions and $0 \leq Energy \leq E_0$ for a set of finite energy signals), then the signal set is trivially convex. Fuzzification can be achieved simply by fuzzifying the interval [139]. Equivalently, fuzzification can be achieved by dilation of the underlying crisp set with a convex dilation kernel. If the dilation kernel is convex, then the dilation result can be interpreted as an α-cut of a fuzzy convex set [102]. The degree of membership of a signal in the fuzzy signal set is equal to that of the membership of the parameter in the fuzzified parameter set.

If the crisp set of functions is not parameterized, fuzzification can be achieved through the direct morphological dilation [141] of each signal in the set. The

α-cuts of the fuzzified convex set can be generated by choosing convex dilation kernels of increasing dimension.

Fuzzification by dilation of convex sets assumes invariance of location of the crisp set in the Hilbert space. However, this may be disadvantageous in certain cases where one of the non-intersecting convex sets is located far away from the other sets. Use of dilation in this case will lead to an unacceptably low α-cut value to enable intersection. Therefore, translation of this set towards the other sets in the Hilbert space, can help maintain an acceptable α-cut value for dilation. This is illustrated in Figure 6.4. It should be noted that such translation of a convex set in the Hilbert space amounts to changing the fundamental characteristics of the *a priori* constraints it represents. Therefore, it can only be performed adaptively, during the POCS iterations.

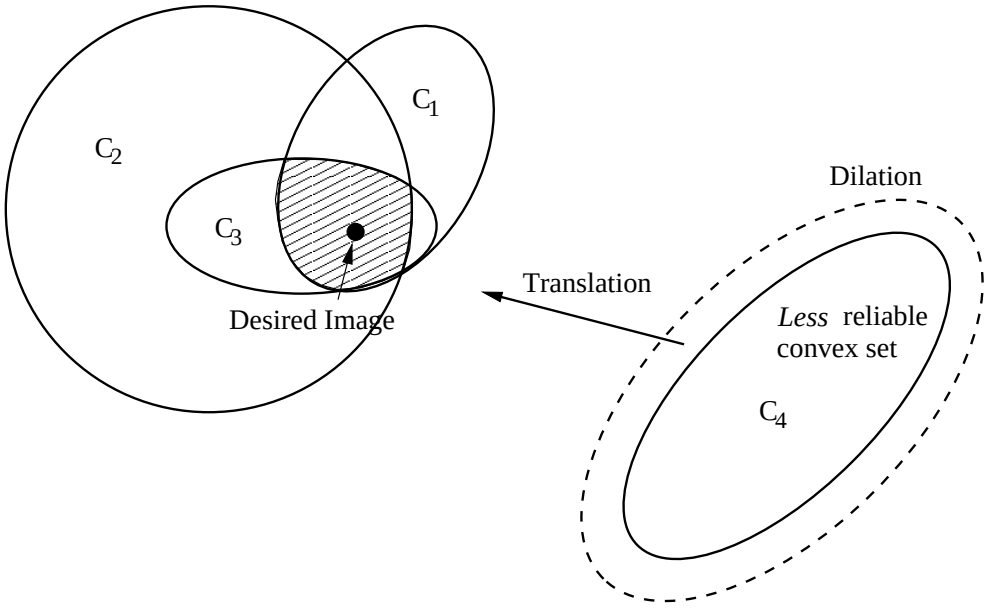

Figure 6.4: Fuzzy POCS involves dilation and translation of *less* reliable convex sets.

Fuzzy POCS of another type can be applied to the case where two or more convex sets intersect in more than one point. It should be noted that such an intersection of two or more convex sets is also inherently convex. Convergence to

interior points of the intersection, if they exist, can be obtained by the application of morphological erosion [141] to one or more convex sets. This is effectively the reverse of fuzzification by dilation, and can be achieved simply by choosing high α-cut values of the fuzzy convex sets. Therefore, convergence would be to a point within rather than on the shaded area, as shown in Figure 6.4. The approach is similar to peeling away convex hulls to find the most interior of a set of points. This particular type of fuzzification is not used in this thesis, since the regularization problem encountered in Chapter 5 is mainly due to non-intersecting convex sets rather than to intersection sets having more than one element.

6.3.1 Fuzzy Convex Sets

Fuzzy convex sets were first introduced by Zadeh in his pioneering work, presented in 1965 [131]. A fuzzy set C_f on the universal set X is defined by the membership function μ_C, which maps X to the real value $[0, 1]$. The fuzzy set C_f can be written as

$$C_f = \{x/\mu_C(x) \quad | \quad x \in X\} \tag{6.1}$$

If ${C_f}^{\alpha}$ denotes the crisp set corresponding to an α-cut of C_f

$${C_f}^{\alpha} = \begin{cases} \{x \quad | \quad \mu_C(x) \geq \alpha, \quad x \in X\} & \text{for} \quad \alpha \neq 0 \\ X & \text{for} \quad \alpha = 0 \end{cases} \tag{6.2}$$

The fuzzy set C_f is considered to be convex, if and only if for every $0 \leq \lambda \leq 1$

$$\mu_C\left[\lambda x_1 + (1-\lambda)x_2\right] \geq min\left\{\mu_C(x_1), \mu_C(x_2)\right\} \tag{6.3}$$

Equivalently, it has been shown that C_f is convex, if all of its α-cuts for $0 \leq \alpha \leq 1$ are convex [131].

Let $m(x,y)$ be an arbitrary image in a Hilbert space $\mathcal{H}$. If the spatial frequency distribution of $m(x,y)$ is denoted by S

$$S = \mathcal{F}\{m(x,y)\} \qquad\qquad m(x,y) \in \mathcal{H} \tag{6.4}$$

where $\mathcal{F}\{.\}$ is the Fourier transform. Let the following constraints on the form of m be known as *a priori* information.

(1) Finite support constraint:

$$\mathcal{C}_1 = \{m(x,y) \quad | \quad m(x,y) = 0 \quad \text{for} \quad (x,y) \notin ROI\} \tag{6.5}$$

where ROI is a pre-specified region of interest. In order to fuzzify this constraint, the boundary of the ROI can be dilated morphologically. The extent of dilation is decided, based on the reliability of the extracted ROI boundary (ie. using the algorithm described in Chapter 2). Another method of dilating the set $\mathcal{C}_1$ would be to introduce a finite maximum energy limit allowable outside the ROI, as given in the following equation.

$$\frac{1}{N^2}\sum_x\sum_y \|m(x,y)\|^2 \leq E_{out} \quad \forall (x,y) \notin ROI \tag{6.6}$$

where E_{out} is the maximum energy allowable outside ROI. The fuzzification parameter E_{out} is estimated using the image with artifacts (i.e. $m'(x,y)$) reconstructed via conventional IFFT method, as shown below

$$E_{out} = 10\% \times \frac{1}{N^2}\sum_x\sum_y \|m'(x,y)\|^2 \quad \forall (x,y) \notin ROI \tag{6.7}$$

(2) Amplitude constraint: If the amplitude values of $m(x,y)$ are known to be restricted within the limits I_{min} and I_{max}, the amplitude constraint is given by

$$\mathcal{C}_2 = \{m(x,y) \quad | \quad I_{min} \leq m(x,y) \leq I_{max} \qquad \forall (x,y)\} \tag{6.8}$$

The set $\mathcal{C}_2$ can be fuzzified through direct fuzzification of the parameters I_{min} and I_{max}. However, for greyscale images it is known that $I_{min} = 0$ and $I_{max} = 255$. Therefore, this set was not fuzzified in the experiments.

(3) Energy constraint: If the total energy within ROI is known to have an upper limit of E_{max}, the energy constraint is given by

$$\mathcal{C}_3 = \{m(x,y) \quad | \quad E = \sum_x \sum_y \|m(x,y)\|^2 \leq E_{max}\} \tag{6.9}$$

where E_{max} is a pre-defined maximum energy limit. Similarly to $\mathcal{C}_2$, $\mathcal{C}_3$ can also be fuzzified by direct fuzzification of the parameter E_{max}. In the experiments, E_{max} was not fuzzified, and set as the total pixel energy of the image with artifacts (i.e. $m'(x,y)$) reconstructed via conventional IFFT method.

Sets $\mathcal{C}_1$, $\mathcal{C}_2$ and $\mathcal{C}_3$ are well established convex sets [103]. Since their fuzzification is achieved via dilation, the resultant α-cuts will also be convex sets. However, it is not essential that *all* the convex sets involved to be fuzzified for fuzzy POCS to work. As indicated above, in the experiments conducted with regard to this thesis, both the $\mathcal{C}_2$ and $\mathcal{C}_3$ sets were not fuzzified.

(4) k-space data constraint: Let $\hat{S}$ denote the partially defined spatial frequency data (i.e. the k-space information) interpolated from the acquired data. Therefore, the k-space constraint can be given by

$$\mathcal{C}_4 = \{m(x,y) \quad | \quad \mathcal{F}\{m(x,y)\} = \hat{S}(k_x,k_y) \quad (k_x,k_y) \in R_0\} \tag{6.10}$$

where R_0 is the region of k-space filled by the computed spatial frequency values. It is also known that $\mathcal{C}_4$ is a convex set of the form of a linear variety [67]. Since each $\hat{S}(k_x,k_y)$ value in R_0 may be affected by interpolation errors (ϵ_1), measurement errors (ϵ_2) and signal noise (ϵ_3), it is possible to define a reliability function (r) for each $(k_x,k_y) \in R_0$.

$$r(k_x,k_y) = f(\epsilon_1,\epsilon_2,\epsilon_3) \tag{6.11}$$

Now a vector space X can be defined, so that if $\vec{x}_i \in X$,

$$\vec{x}_i = \mathcal{F}^{-1} \begin{cases} \hat{S}(k_x,k_y) & \text{for some } (k_x,k_y) \in R_0 \\ 0 & \text{otherwise} \end{cases} \tag{6.12}$$

Therefore, the k-space of $\vec{x}_i$ consists of a single non-zero value at $(k_x, k_y) \in R_0$. If there are p non-zero values in $\hat{S}$, X will consist of p vectors, hence $i = 1, 2, ..., p$. Each vector $\vec{x}_i \in X$ is associated with a reliability function r_i which can be mapped to $[0, 1]$ to create a membership function $\mu(\vec{x}_i)$. Hence, it is possible to define the following fuzzy set $\mathcal{C}_f$ [115]

$$\mathcal{C}_f = \{(\vec{x}_i, \mu(\vec{x}_i)) | \vec{x}_i \in X\} \tag{6.13}$$

Lemma 1: The linear variety V given by the convex set $\mathcal{C}_4$ is represented by the vectors $\vec{x}_i \in \mathcal{C}_f$.

Proof: Let $\vec{m}_0 \in V$. Then the image represented by the vector $\vec{m}_0$ is given by $m_0(x, y)$ where

$$\mathcal{F}\{m_0(x,y)\} = \begin{cases} \hat{S}(k_x, k_y) & \forall (k_x, k_y) \in R_0 \\ 0 & \text{otherwise} \end{cases}$$

Inverse Fourier transform for $(k_x, k_y) \in R_0$ gives

$$m_0(x,y) = \frac{1}{N} \sum_{k_x} \sum_{k_y} \hat{S}(k_x, k_y) \exp\left[i \frac{2\pi}{N}(xk_x + yk_y)\right] \tag{6.14}$$

Since there are p non-zero values within the region R_0, using the linearity of the inverse Fourier transform

$$m_0(x,y) = \mathcal{F}^{-1}\{\hat{S}(k_x, k_y)_1\} + ... + \mathcal{F}^{-1}\{\hat{S}(k_x, k_y)_p\} \tag{6.15}$$

From the definition in Equation 6.12,

$$\vec{m}_0 = \vec{x}_1 + \vec{x}_2 + ... + \vec{x}_p = \sum_{i=1}^{p} \vec{x}_i \qquad \vec{x}_i \in \mathcal{C}_f \tag{6.16}$$

Therefore, $\vec{m}_0 = \sum_{i=1}^{p} \vec{x}_i \in V$. Since V can be represented by a unique subspace translated by the vector $\vec{m}_0$ where $\vec{m}_0 \in V$, from the result in Equation 6.16,

$$V = \sum_{i=1}^{p} \vec{x}_i + M \tag{6.17}$$

where M is the unique subspace in $\mathcal{H}$. Therefore, the linear variety V can be represented in terms of the vectors $\vec{x}_i \in \mathcal{C}_f$.

- Q.E.D.

Lemma 2: Let X be a vector space $X = \{\vec{x}_1, \vec{x}_2, ..., \vec{x}_p\}$ and S be a proper subset of X. If $V_X = \sum_{i=1}^{p} \vec{x}_i + M$ where $\vec{x}_i \in X$ and $V_S = \sum_{i=1}^{k} \vec{x}_i + N$ where $\vec{x}_i \in S \subset X$, then N is a dilated subspace of M.

Proof: Since S is a proper subset of X, $k < p$. Therefore, from *Lemma 1*

$$V_X = \sum_{i=1}^{k} \vec{x}_i + \sum_{i=k+1}^{p} \vec{x}_i + M \tag{6.18}$$

for $\vec{x}_i \notin M$ by the definition of a linear variety [108].

Let $\bar{x} = \sum_{i=1}^{k} \vec{x}_i$. Therefore, $V_X = \bar{x} + (M + \sum_{i=k+1}^{p} \vec{x}_i)$ and $V_S = \bar{x} + N$. Let the subspace generated by the vector space $\{\vec{x}_{k+1}, \vec{x}_{k+2}, ..., \vec{x}_p\}$ be G. If we let $V_X \equiv V_S$, then $N \equiv M \bigcup G$. Therefore, if M is the subspace generated by vector space $S_M = \{\vec{y}_1, ..., \vec{y}_n\}$, then N is the subspace generated by vector space $S_N = \{\vec{y}_1, ..., \vec{y}_n, \vec{x}_{k+1}, ..., \vec{x}_p\}$. Hence, $S_M \subset S_N$, which proves that N is a dilated subspace of M.

- Q.E.D.

From *Lemma 2*, it is possible to dilate the subspace M by decreasing the number of elements in X.

If $\mathcal{C}_1 \bigcap \mathcal{C}_4 = \{\phi\}$, POCS does not converges to a solution in $\mathcal{C}_1$. Instead of $\mathcal{C}_4$, if we use $\mathcal{C}_f$ with an appropriate α-cut, so that

$$\mathcal{C}_f{}^{\alpha} = \{\vec{x} \quad | \quad \mu(\vec{x}) \geq \alpha \quad \vec{x} \in X\} \tag{6.19}$$

it may be possible to find $\mathcal{C}_1 \bigcap \mathcal{C}_f{}^{\alpha} \neq \{\phi\}$, since according to *Lemma 2* the corresponding subspace can be appropriately dilated until an intersection between $\mathcal{C}_1$

and ${\mathcal{C}_f}^{\alpha}$ occurs. If not, at least the minimum distance between $\mathcal{C}_1$ and the linear variety ${\mathcal{C}_f}^{\alpha}$ can be reduced producing a *closer* solution to the set $\mathcal{C}_1$.

6.3.2 Estimation of α-cut Value

Let $\vec{a}$ be the vector representation of the image $m(x, y)$ of size $N \times N$. The l^{th} element of $\vec{a}$ can be given as in Equation 6.20.

$$a_l = m\left(REM\left[\frac{l}{N}\right], INT\left[\frac{l}{N}\right] + 1\right) \tag{6.20}$$

where $l = 0, 1, ..., N^2 - 1$. $REM\left[\frac{l}{N}\right]$ represents the remainder when l is divided by N, and $INT\left[\frac{l}{N}\right]$ represents the integer part when l is divided by N. If there are N_a elements outside the ROI, N_a elements in $\vec{a}$ are known *a priori*, out of the total N^2 elements.

Similarly, let $\vec{b}$ be the vector representation of the k-space data $S(k_x, k_y)$ of size $N \times N$. The k^{th} element of $\vec{b}$ can be given as in Equation 6.21.

$$b_k = S\left(REM\left[\frac{k}{N}\right], INT\left[\frac{k}{N}\right] + 1\right) \tag{6.21}$$

where $k = 0, 1, ..., N^2 - 1$. $REM\left[\frac{k}{N}\right]$ and $INT\left[\frac{k}{N}\right]$ have similar definitions to that of Equation 6.20. If there are N_b values in R_o regions of the k-space, it is possible to formulate a system of linear equations consisting of N_b number of equations.

Therefore, the general equation that relates k-space values to the MR image (see Equation 2.23 of Chapter 2 Section 2.5) can be written in matrix form as shown in Equation 6.22.

$$Q\vec{a} = \vec{b} \tag{6.22}$$

where $Q = \{q_{lk}\}$ is the known matrix of Fourier coefficients. where q_{lk} is given by

$$q_{lk} = \exp\left\{-j\frac{2\pi}{N}\left[REM\left[\frac{l}{N}\right] REM\left[\frac{k}{N}\right] + \left(INT\left[\frac{l}{N}\right] + 1\right)\left(INT\left[\frac{k}{N}\right] + 1\right)\right]\right\} \tag{6.23}$$

where $l = 0, 1, ..., N^2 - 1$ and $k = 0, 1, ..., N^2 - 1$. By solving this system of equations, the target is to estimate the unknown $(N^2 - N_a)$ elements in $\vec{a}$. In order to achieve this target, it is possible to use maximum of N_b available equations, formed using the known values in the data filled R_o regions of the k-space.

If $N_b < (N^2 - N_a)$, number of unknowns are greater than the number of equations. Therefore, there can be infinite number of possible solutions, and our target cannot be achieved.

If $N_b > (N^2 - N_a)$, a solution can be found if the system of equations is consistent. However, due to noise and interpolation errors, this system of equations is almost always inconsistent. Therefore, in order to force a solution, it is required to choose only $(N^2 - N_a)$ equations out of the available N_b equations. When selecting these equations, it is advantageous to choose the most reliable equations, in order to obtain a more accurate solution. These equations can be attached a reliability measure equivalent to the membership of the k-space value used to generate each equation. Now it is possible to construct a crisp set of equations by selecting an α-cut value which ensures only $(N^2 - N_a)$ equations are contained within the selected set. Therefore, if $N_b > (N^2 - N_a)$, the α-cut for ${C_f}^{\alpha}$ is calculated so that the resulting crisp set contains $(N^2 - N_a)$ elements. The above estimation assumes that the resulting system of linear equations contains no singularities.

6.4 Fuzzy Data Model

It is possible to define a fuzzy set so that its membership function can be seen as a possibility distribution. The information from a specialist, expressed by "about $\beta \approx A$", is replaced by $\mu_A(x)$, where this new expression is taken as the information that expresses the possibility of A being in the vicinity of β [137].

Therefore, a fuzzy number A is expressed as $A = (\beta, c)$, where β expresses the centre of the region of possibility and c its spread. The membership function of A can be given by

$$\mu_A(x) = L\left(\frac{x-\beta}{c}\right) \qquad c > 0 \tag{6.24}$$

where $L(x)$ is called the reference function [137] and possesses the following properties:

- $L(x) = L(-x)$
- $L(0) = 1$
- $L(x)$ is a strictly decreasing function for $[0, \infty)$.

Examples of $L(x)$ for $p > 0$ are functions such that $L_1(x) = max(0, 1 - |x|^p)$, $L_2(x) = e^{-|x|^p}$ etc. If $L_1(x)$ is considered for $p = 1$, the result is a triangular fuzzy number as depicted in Figure 6.5.

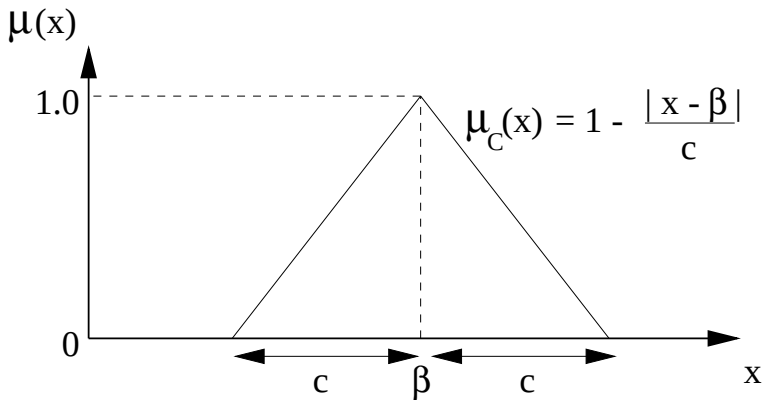

Figure 6.5: $\mu_C(x)$ of a triangular fuzzy number.

The major obstacle to the fuzzification of k-space data is the estimation of the spread (c) of the possibility function. Since each spatial frequency value is subjected to differing measurement errors, interpolation errors and noise, the overall effect of such errors is highly complex and difficult to accurately model as a general rule. However, it is possible to identify pairs of complex conjugate k-space

points, since $|S(k_x, k_y)| \approx |S^*(N-k_x, N-k_y)|$, where $S^*(\cdot)$ indicates the complex conjugate and N is the number of phase encoding (k_y) or frequency encoding (k_x) steps. Although the phase of these alleged complex conjugate values can be corrupted due to acquisition timing, the magnitudes should generally be matched within an error limit.

If the re-gridded k-space provides $p\left[< N(\frac{N}{2}-1)\right]$ conjugate pairs of interpolated data, it is possible to determine the spread of the possibility function based on the difference of the magnitudes of the conjugate pairs, leading to triangular fuzzy models for each element S_1 and S_2, as shown in Figure 6.6.

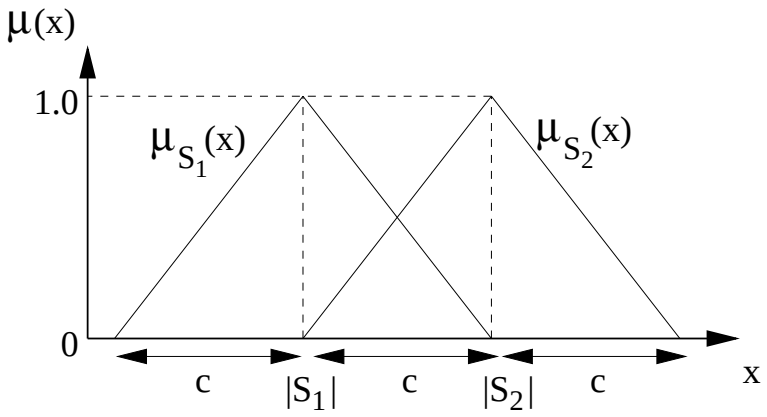

Figure 6.6: Membership functions of a conjugate pair.

The separation between $|S_1|$ and $|S_2|$ in fact represents the spread of the possibility function, since the "closeness" of the values $|S_1|$ and $|S_2|$ indicates a higher possibility of both $|S_1|$ and $|S_2|$ being "closer" to the uncorrupted k-space value. The noise corruption and interpolation errors cause $|S_1|$ and $|S_2|$ to be different, and this difference approximately indicates the reliability of the data. The higher the difference, the less reliable the data will be. However, it is possible that one of the numbers in the conjugate pair is "closer" to the uncorrupted value than the other. This information will not be apparent in the possibility spread. Therefore, the fuzzy model describes the composite reliability of the conjugate pair rather than the reliability of individual elements. Hence, the membership

functions of S_1 and S_2 can be combined to provide a composite membership function ($[\mu_S(x)]$) for the conjugate pair, as given in Equation 6.25.

$$\mu_S(x) = min\{1, \mu_{S_1}(x) + \mu_{S_2}(x)\} \tag{6.25}$$

6.5 Regularization using Fuzzy POCS

The reason for fuzzification of k-space data is primarily to provide soft k-space constraints during the POCS iterations. Hence, the algorithm takes the form of a simple fuzzy dynamic program, in which the "decision points" include varying degrees of fuzziness or ambiguity [137]. Since POCS iterations do not converge to the k-space elements at the same rate, fuzzy rules are proposed for the "decision points" based on the convergence rate of each k-space element and the overall convergence rate of POCS.

- Rule 1: Let the k-space values for a fuzzy conjugate pair at the n^{th} iteration be S_n and $S^*{}_n$. Let e_0 be a "very small" value. If $\frac{||S_n|-|S_{n-1}||}{|S|} < e_0$ and $\mu_S(|S_n|) = 0$, then the corresponding values are removed from the k-space constraints due to a high degree of unreliability. The vacant k-space points are added to the set of values to be estimated during consequent POCS iterations.

- Rule 2: If $||S_n|-|S|| < \rho$, the corresponding values are preserved as k-space constraints due to a high degree of reliability. S represents the k-space data in R_o generated by the algorithm described in Chapter 5. ρ is a small fuzzy limit with its membership function mapped from the overall convergence rate of the POCS algorithm. Let the error outside the region of interest (ROI) for the reconstructed image at the n^{th} iteration be E_n. A measure of the convergence rate ζ_n is defined as follows:

$$\zeta_n = log_{10}(E_{n-1} - E_n) \tag{6.26}$$

Note that $E_{n-1} > E_n$ for all n, since the POCS algorithm is converging. Therefore, ζ_n exists for all n. The membership function of ρ is given by

$$\mu_\rho(\zeta_n) = \begin{cases} 1.0 & \text{for } \zeta_n \geq 0.0 \\ e^{-\frac{|\zeta_n|^2}{4}} & \text{for } \zeta_n < 0.0 \end{cases} \tag{6.27}$$

Hence, $\rho = r_0 \mu_\rho(\zeta_n)$ where r_0 is a "small" number.

- Rule 3: If $\frac{||S_n|-|S_{n-1}||}{|S|} < e_0$, $||S_n| - |S|| > \rho$ and $\mu_S(|S_n|) > 0$, then the original k-space values are updated to the new values at the n^{th} iteration, and preserved as k-space constraints.

According to the above rules, the new value for a particular k-space value in R_o can be given as in Equation 6.28

$$S_n(k_x, k_y) = \begin{cases} 0 & \text{under Rule 1, and} \\ & (k_x, k_y) \text{ removed from } R_o \\ S(k_x, k_y) & \text{under Rule 2} \\ S_{n-1}(k_x, k_y) & \text{under Rule 3} \end{cases} \tag{6.28}$$

6.6 Simulation Results

In order to test the effectiveness of the proposed fuzzy algorithm, several simulation studies are performed. The same data sets as those given in Chapter 5 Figure 5.3 are used, due to the ease of comparing the results. The Shepp and Logan phantom [121] is used in the simulations. Results of using the proposed algorithm on real MR head images are also included towards the end of this Section.

Firstly, the Fuzzy POCS algorithm is tested using the noise free data of cases 1 and 2, assuming accurate measurements of rotation angels. Therefore, the available k-space values are only subjected to interpolation errors. The parameters

(a)

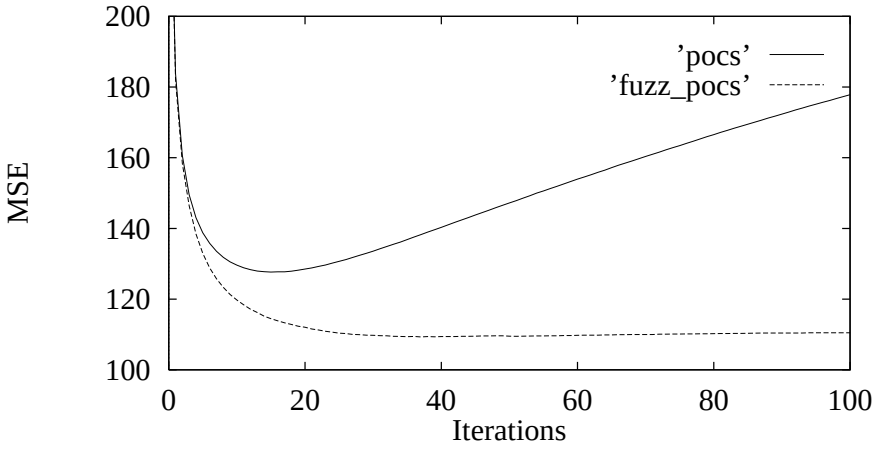

(b)

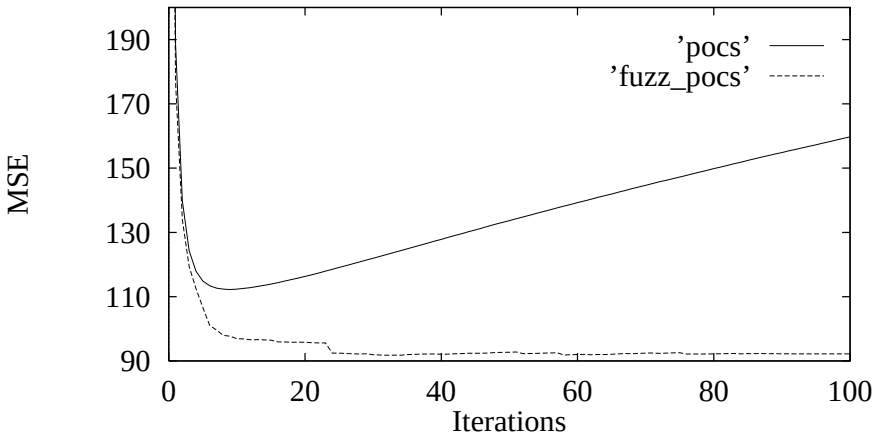

Figure 6.7: Comparison of MSE for 100 iterations of POCS and Fuzzy POCS algorithms: (a) Case 1; (b) Case 2.

used for iterations are $e_0 = 0.005$ and $r_0 = 0.2$. The results are compared to the method involving conventional POCS, as shown in Figures 6.7(a) and 6.7(b). A relative measure on the quality of the reconstructed image is obtained using the mean squared error (MSE), which is defined by

$$MSE = \frac{1}{N^2} \sum_{x=0}^{N-1} \sum_{y=0}^{N-1} [m_{2j}(x,y) - m(x,y)]^2 \tag{6.29}$$

where $m_{2j}(x,y)$ is the reconstructed image at the j^{th} iteration and $m(x,y)$ represents the original image. It should be noted that in practice, $m(x,y)$ is unknown and hence the MSE value is unavailable.

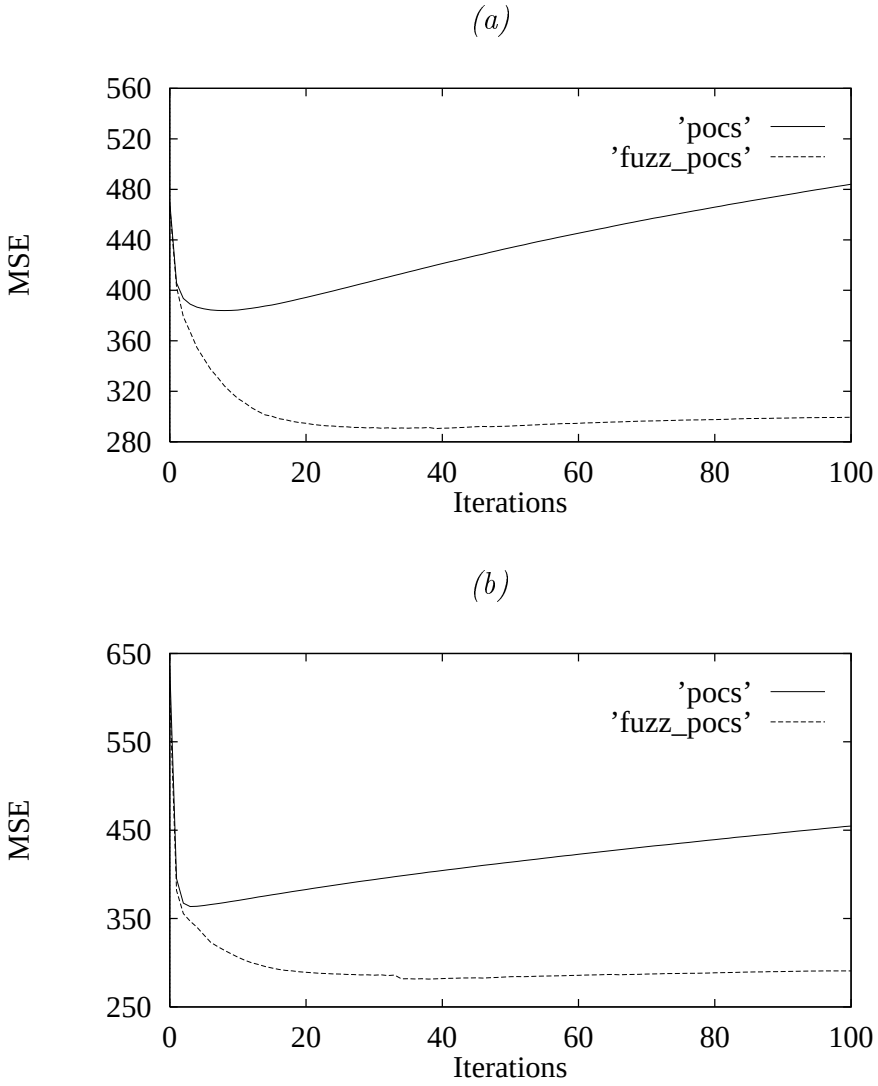

Figure 6.8: Comparison of MSE for 100 iterations of POCS and Fuzzy POCS algorithms, for noisy data ($SNR = 10dB$): (a) Case 1; (b) Case 2.

Figures 6.8(a) and 6.8(b) show the relative performance of the proposed method compared to conventional POCS, for cases 1 and 2 with introduced Gaussian noise at $SNR = 10dB$. It can be clearly seen that with conventional POCS, the reconstructed image diverges from the desired image after a finite number of iterations. Since the MSE measure is unavailable, the conventional POCS method has to rely on a computationally complex and highly time consuming *regulatory error metric* (see Chapter 5) in order to find the optimum point to terminate the iterations. With the proposed algorithm, iterations can be terminated when E_n

reaches a desired limit without compromising the quality of the image, due to the avoidance of divergence.

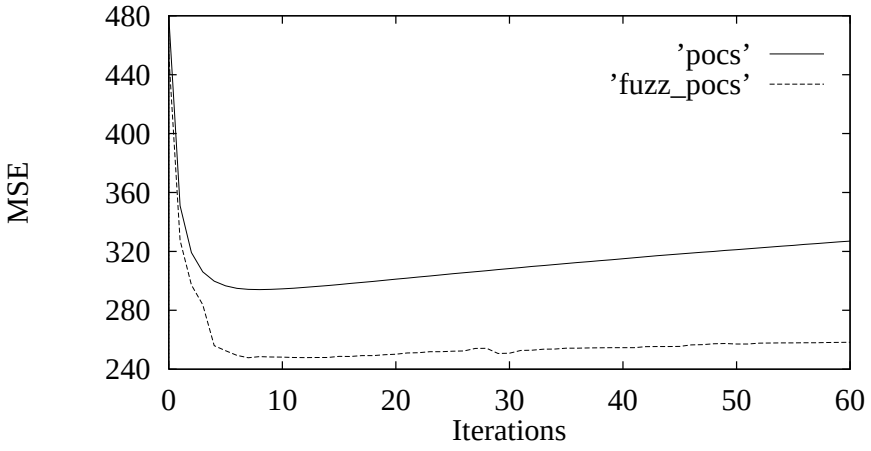

Figure 6.9: Comparison of MSE for 60 iterations of POCS and Fuzzy POCS algorithms, for data with measurement errors - Case 3.

The data set in Case 3 is used to test the algorithm for continuous motion with $\pm 1^o$ errors in rotation angle measurements. Therefore, the available k-space values were only subjected to interpolation and measurement errors. Figure 6.9 shows the relative performance of Fuzzy POCS compared to conventional POCS.

Figure 6.10 shows the reconstructed images using conventional POCS after 60 iterations for Cases 1 and 3 respectively, whereas Figure 6.11 shows the corresponding results using the proposed algorithm after the same number of iterations. Due to the regularization using Fuzzy POCS, it is evident that the artifacts shown in Figure 6.10 are better suppressed in the results shown in Figure 6.11.

Shepp & Logan phantom is primarily used due to the ease of objective quantification of the research results. However, the algorithm proposed in this chapter can equally well be applied to real MR images as shown in Figures 6.12 and 6.13 for axial and sagittal head images respectively. These images are reconstructed using all the methods described in this thesis including ROI extraction, rotational motion parameter estimation and fuzzy POCS based k-space data correction.

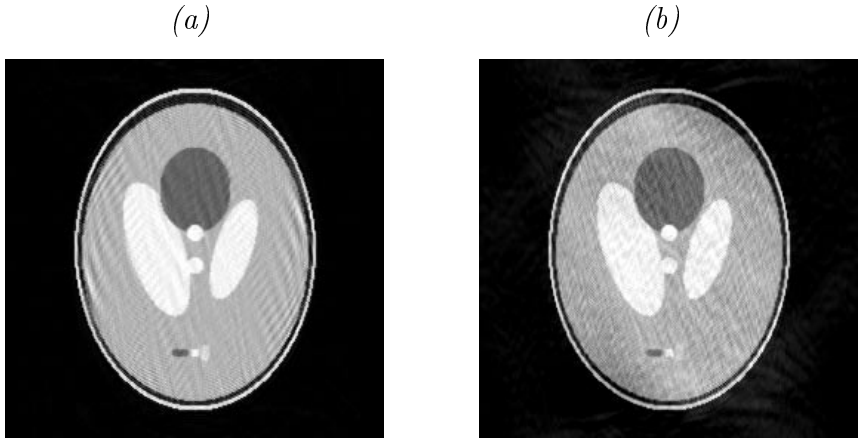

Figure 6.10: Reconstructed images from data sets in Case 1 and Case 3, after 60 iterations, using POCS: *(a)* Case 1 ($MSE = 153.943$); *(b)* Case 3 ($MSE = 327.025$)

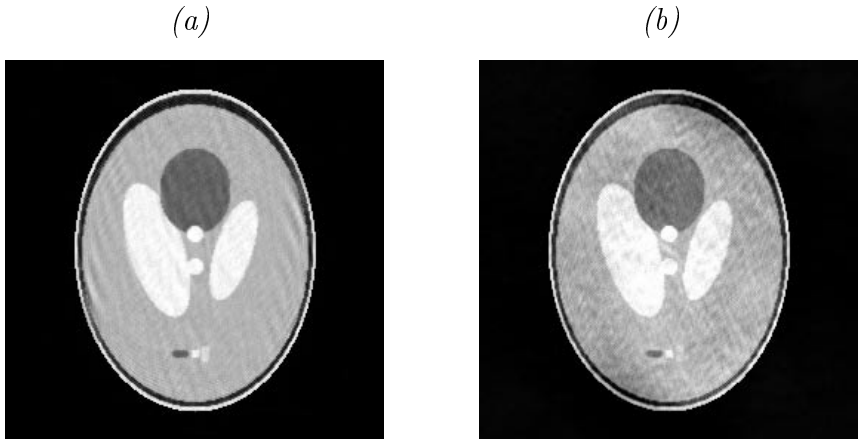

Figure 6.11: Reconstructed images from data sets in Case 1 and Case 3, after 60 iterations, using Fuzzy POCS: *(a)* Case 1 ($MSE = 109.769$); *(b)* Case 3 ($MSE = 258.261$)

To put these results into perspective, the corrected images are compared to the images reconstructed using conventional IFFT.

The α-cut values used in the fuzzy POCS algorithm (see Section 6.3.2) for the above experiments are shown in Table 6.1. The number of pixels outside the ROI and the number of retained k-space values in R_o region (see Section 6.3.1 Equation 6.12) are also indicated for each case studied.

It should be noted that the choice of e_0 and r_0 are not optimized for the above simulations. Further simulations are performed in order to study the effect of

(a) *(b)*

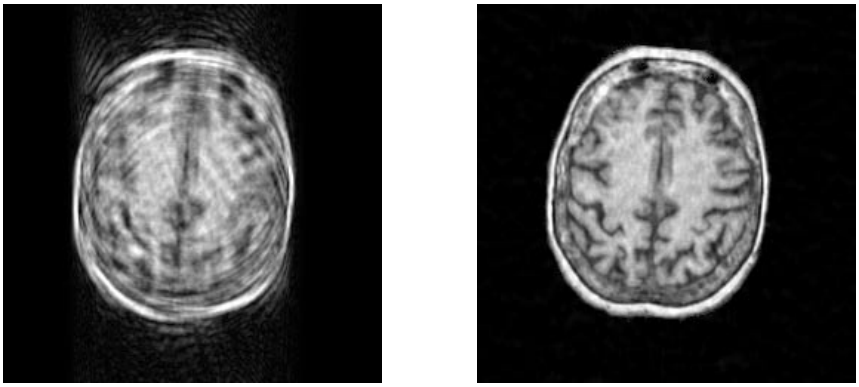

Figure 6.12: Reconstructed MR image comparison for an axial head image: *(a)* using conventional IFFT method ($MSE = 1147.2$); *(b)* using the methods proposed in this thesis ($MSE = 86.5$)

(a) *(b)*

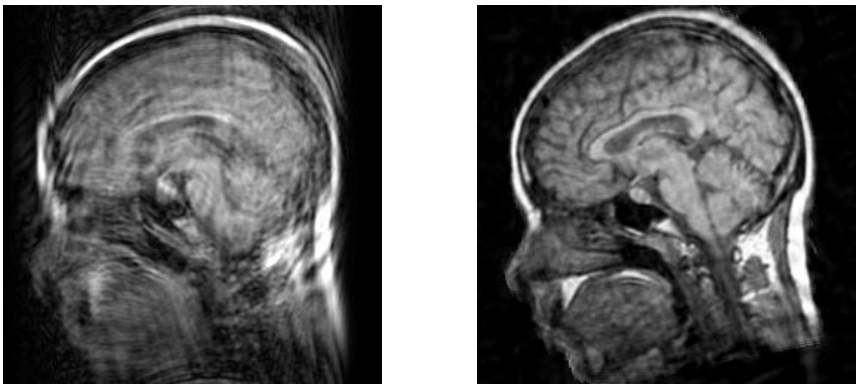

Figure 6.13: Reconstructed MR image comparison for a sagittal head image: *(a)* using conventional IFFT method ($MSE = 2640.1$); *(b)* using the methods proposed in this thesis ($MSE = 408.7$)

the choice of e_0 and r_0. The MSE values are recorded after 60 iterations using the data set in Case 1 with noise ($SNR = 10dB$) and without noise, for various values of the above parameters. The results are presented in Figures 6.14(a) and 6.14(b) respectively.

The parameter e_0 can be considered as a relaxation parameter for the convex set $\mathcal{C}_4$, which enables the available k-space values to change during the POCS iterations, where the extent of allowable change is governed by e_0. Higher values of e_0 provide greater freedom of change for the k-space values, hence the final

Experiment	α-cut value	number of pixels outside ROI (N_a)	number of retained k-space values (N_b)
Case 1	0.25	37629	51823
Case 2	0.22	37629	46058
Axial	0.38	45083	50907
Sagittal	0.20	25101	53895

Table 6.1: The α-cut values used in the fuzzy POCS algorithm. The number of pixels outside the ROI (N_a) and the number of retained k-space values in R_o region (N_b) are also indicated for each case studied.

POCS solution is less dependent on the available k-space constraints than the spatial constraints given by the convex sets $\mathcal{C}_1$ to $\mathcal{C}_3$. Therefore, if the available k-space data are less reliable due to measurement errors or noise, the choice for e_0 should be comparatively large within the interval $[0, 1]$. The information on the signal-to-noise ratio (SNR) can be obtained directly from the MRI scanner, whereas the angle measurement accuracy depends on the estimation reliability $\mu[\theta_{est}(k_m)]$ from the algorithm described in Chapter 4. If the available k-space values are only subjected to interpolation errors, a choice of small e_0 will produce a higher quality final image, since the k-space constraints are sufficiently reliable in order to drive the POCS solution towards the required solution. The above claim is supported by the results shown in Figure 6.14(a).

The fuzzy parameter ρ can be viewed as a feedback parameter, which base the decision to change a particular k-space value on the error reduction rate outside the ROI. The parameter r_0 controls the effect of this feedback. A lower value for ρ indicates a drop in the error reduction rate. Therefore, the algorithm reacts by giving more freedom of change for the k-space values in order to expedite this rate. Assigning a lower value for r_0 simulates a sluggish error reduction rate, hence forcing the algorithm to relax the k-space constraints. Therefore, a "very small" value for r_0 is desirable only if the available k-space data are affected by

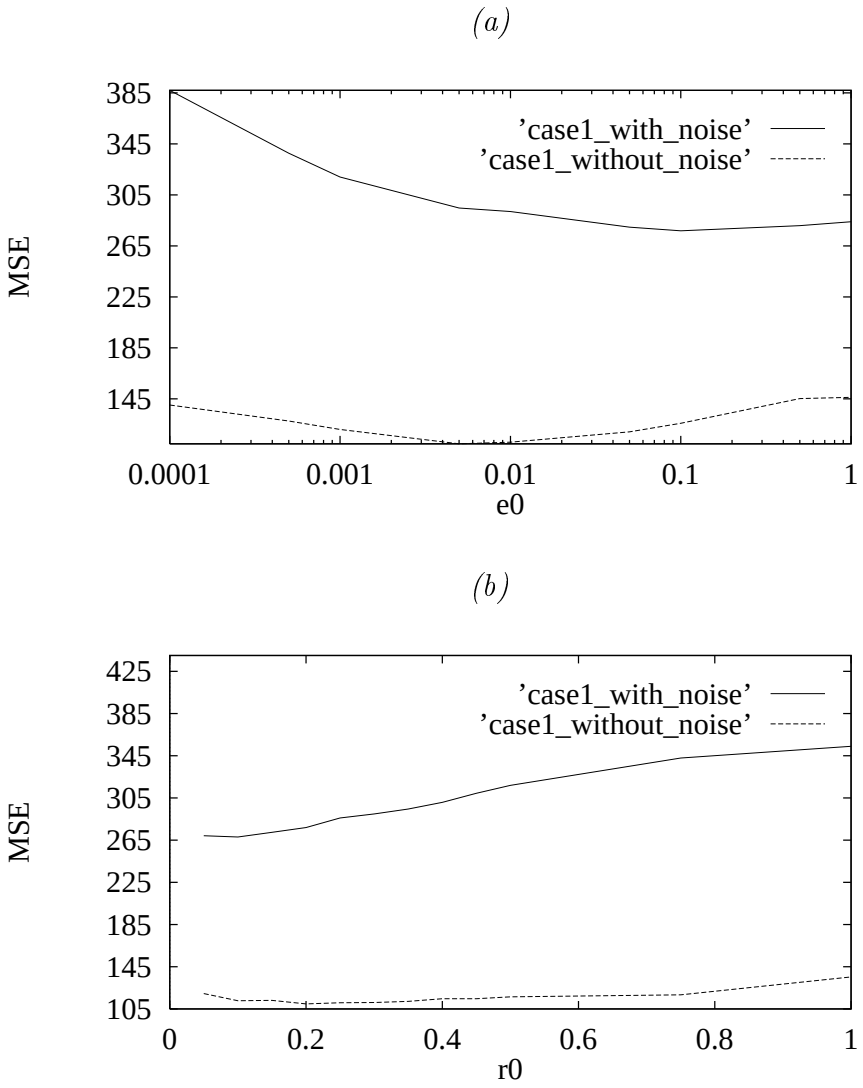

Figure 6.14: Optimization of Fuzzy POCS parameters for Case 1, with ($SNR = 10dB$) and without noise: (a) relaxation parameter e_0; (b) feedback control parameter r_0.

noise and measurement errors. However, in order to avoid divergence, the value of r_0 should remain within the interval $[0.1, 0.35]$, as shown in Figure 6.14(b).

The computation time for the motion artifact correction technique proposed in this thesis is an important issue. Therefore, the total time required (typically) to correct an image is given in Table 6.2, with a breakdown of where the time taken.

Notice that the typical correction times are based on the average value of the time

Task	Typical time required (min.)
Boundary extraction	5.2
Rotation angle estimation	148.7
K-space data correction	8.2
Missing data estimation and image reconstruction	6.7
Total time	168.8

Table 6.2: The total time required (typically) to correct an image is given, with a breakdown of where the time taken.

taken in the 6 cases studied in this thesis. The ROI boundary extraction includes view selection, fuzzy model implementation and snake energy minimization. The rotation angle estimation includes computing X-directional IFT, estimation of X-directional IFT width using two open snake contours, creation of a look-up table, calculating initial guesses and improving these initial values using similarity criterion. The k-space data correction includes weighted averaging of overlap data and computing the fuzzy membership of conjugate pairs. Finally, the missing data estimation includes estimation of missing data using fuzzy POCS and the final image reconstruction.

For the six cases described in Chapter 4, the total time ranged from 137 minutes to 182 minutes. It is obvious from Table 6.2 that most time consuming processing step is the motion parameter estimation stage, which accounts for over 85% of the total time. Therefore, the total processing time can be significantly improved by developing efficient motion parameter estimation schemes such as the one described in Chapter 4 of this thesis. It should be noted that according to previously published work [78], this motion estimation step has required over 4.5 hours (270 minutes) for 10 angle estimations, whereas the proposed method requires only 150 minutes for 190 angle estimations. Therefore, it is concluded that the method proposed in this thesis has significantly reduced the total processing time.

6.7 Summary

The original contributions discussed in this chapter are the introduction of a k-space fuzzy data model to represent the reliability of the interpolated k-space data and the development of Fuzzy POCS algorithm to regulate the image reconstruction algorithm. The simulation results indicate that the proposed algorithm is capable of avoiding the divergence of the reconstructed image from the desired image. Appropriate choice of Fuzzy POCS parameters enable successful reconstruction of images from either noise free or noisy MR signals. An additional advantage of the proposed algorithm is that it also avoids the necessity of computing a complicated and highly time consuming regulatory error metric E to determine the point of termination of iterations. The proposed algorithm also ensures final image quality improvement compared to the results obtained via the application of the conventional POCS algorithm.